# The Onset and Interannual Variability of the Asian Summer Monsoon in Relation to Land–Sea Thermal Contrast

CHENGFENG LI AND MICHIO YANAI

*Department of Atmospheric Sciences, University of California at Los Angeles, Los Angeles, California*

(Manuscript received 21 December 1994, in final form 10 July 1995)

ABSTRACT

The onset and interannual variability of the Asian summer monsoon in relation to land–sea thermal contrast and its contributing factors are studied using a 14-yr (1979–1992) dataset. The onset of the Asian summer monsoon is concurrent with the reversal of meridional temperature gradient in the upper troposphere south of the Tibetan Plateau. The reversal is the result of large temperature increases in May to June over Eurasia centered on the Plateau with no appreciable temperature change over the Indian Ocean. In spring the Tibetan Plateau is a heat source that is distinctly separate from the heat source associated with the rain belt in the equatorial Indian Ocean. The Tibetan heat source is mainly contributed by sensible heat flux from the ground surface, while the oceanic heat source is due to the release of latent heat of condensation. It is the sensible heating over the Plateau region in spring that leads to the reversal of meridional temperature gradient. Despite its intensity the condensational heating over the Indian Ocean does not result in tropospheric warming because it is offset by the adiabatic cooling of ascending air.

A monsoon intensity index, based on the magnitude of the summer mean vertical shear of zonal wind over the North Indian Ocean, is used to compare the years of strong and weak Asian summer monsoon circulation. The strong (weak) Asian summer monsoon years are associated with (a) positive (negative) tropospheric temperature anomalies over Eurasia, but negative (positive) temperature anomalies over the Indian Ocean and the eastern Pacific; (b) negative (positive) SST anomalies in the equatorial eastern Pacific, Arabian Sea, Bay of Bengal, and South China Sea, but positive (negative) SST anomalies in the equatorial western Pacific; and (c) strong (weak) heating and cumulus convection over the Asian monsoon region and the western Pacific, but weaker (stronger) heating and convection in the equatorial Pacific.

## 1. Introduction

The Asian summer monsoon as a major component of the global climate system has received renewed attention in recent years. Studies of the global distributions of the mean-tropospheric heating rate elucidated the seasonal migration of heat sources on planetary scale (e.g., Wei et al. 1983; Johnson et al. 1985; Schaack et al. 1990; Schaack and Johnson 1994; Trenberth and Solomon 1994). Schaack and Johnson (1994) showed that in July the heating maximum is located over the northern Bay of Bengal, indicating large contributions from the released latent heat of condensation with monsoonal rains. However, these studies did not examine the differential heating that generates and maintains the large-scale land–sea thermal contrast that is responsible for the movement of the monsoonal rain belt.

The general circulation over Asia undergoes abrupt seasonal changes during late spring or early summer, which are related to the tropospheric warming over the Asian land mass (Murakami and Ding 1982; Krishnamurti 1985; He et al. 1987; Yanai et al. 1992). The significance of the Tibetan Plateau as an elevated heat source for the abrupt seasonal change has been discussed by many authors (e.g., Flohn 1957, 1960; Ye and Gao 1979; Gao et al. 1981; Ye 1981; Luo and Yanai 1984; Murakami 1987; Yanai et al. 1992; Yanai and Li 1994a). Flohn (1957, 1960) suggested that the seasonal heating of the elevated surface of the Tibetan Plateau and the consequent reversal of the meridional temperature and pressure gradients south of 35°N trigger the large-scale change of the general circulation over Asia and the monsoon burst over the Indian subcontinent. Fu and Fletcher (1985) showed that the interannual variability of Indian monsoon rainfall was highly correlated with that of the thermal contrast between the Tibetan Plateau and the equatorial Pacific.

He et al. (1987) showed that, from spring to summer 1979, the general circulation over Asia underwent two distinct stages of abrupt transitions, resulting in the successive onsets of the early summer rains over Southeast Asia and the Indian summer monsoon. The two transitions were related to similar two successive stages of upper-tropospheric warming over longitudes east of

*Corresponding author address:* Dr. Michio Yanai, Department of Atmospheric Sciences, University of California, Los Angeles, 405 Hilgard Avenue, Los Angeles, CA 90095-1565.
E-mail: yanai@atmos.ucla.edu

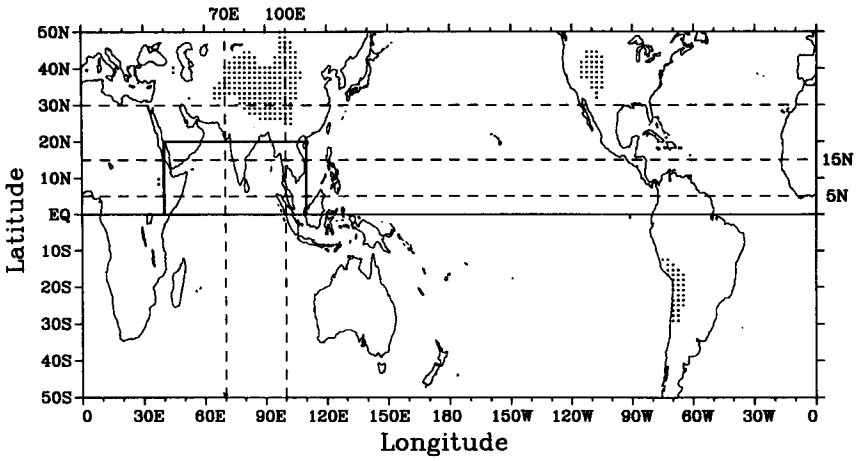


FIG. 1. The map of the analysis domain. The ground surfaces above 1500 m are shaded. The boxed region is chosen to define the Asian summer monsoon intensity index. Time sections along the latitudes and longitudes shown by dashed lines appear in this paper.

85°E (the eastern Tibetan Plateau, South China) and over longitudes west of 85°E (Iran, Afghanistan, the western Tibetan Plateau). The successive warming over these land regions was the primary cause of the successive reversals of the meridional temperature gradient on the south sides of these regions. Yanai et al. (1992) showed that the first stage of upper-tropospheric warming was primarily caused by diabatic heating and warm horizontal advection and the second stage was caused by adiabatic warming due to large-scale subsidence.

The Asian summer monsoon exhibits a considerable interannual variability. This is clearly manifested by year-to-year variations of monsoon rainfall over India (e.g., Parthasarathy and Mooley 1978; Bhalme and Mooley 1980; Sontakke et al. 1993). The interannual variability of the Asian summer monsoon has been related with the El Niño–Southern Oscillation (ENSO) phenomenon. Many studies have shown that El Niño and La Niña are, respectively, associated with the below and above normal Indian summer monsoon rainfall (e.g., Angell 1981; Rasmusson and Carpenter 1983). Barnett (1983, 1984a) found that the monsoon is strongly coupled with the Pacific trade wind system. Barnett (1984b) concluded that the Southern Oscillation, El Niño and climatic variations in the monsoon system are all part of one global-scale phenomenon. Several authors have suggested that the Asian summer monsoon plays active, not passive, roles in its interaction with the El Niño–Southern Oscillation (ENSO) phenomenon (e.g., Meehl 1987; Yasunari 1990, 1991; Webster and Yang 1992).

The years of "strong" and "weak" Asian monsoon have been studied in relation to the variation of the atmosphere/ocean circulation system in the tropical Indian Ocean and Pacific sectors (e.g., Meehl 1987; Webster and Yang 1992). Meehl (1987), using the Indian monsoon rainfall as an index of monsoon intensity, classified the summer monsoon seasons since 1890 as either strong or weak season. He showed that a year with strong Indian monsoon is characterized by warm SSTs and enhanced convection to the west of the South Pacific convergence zone (SPCZ), but decreased precipitation and cold SSTs to the east of the SPCZ. A weak monsoon year is characterized by warm SSTs in the tropical eastern Pacific. He suggested that the tropical east–west circulation in the Asian/Pacific sector provides a connection between the Asian summer monsoon and ENSO. Krishnamurti et al. (1989, 1990) documented contrasting conditions of the monsoon system for 1987 and 1988, which are classified as a weak and a strong monsoon, respectively, in terms of the Indian monsoon rainfall. In another approach, Webster and Yang (1992) classified the Asian monsoon seasons since 1968 as either strong or weak monsoon seasons by the intensity of vertical shear of zonal wind in the Asian monsoon region in summer. Their results showed that a strong monsoon season is associated with enhanced summer trade winds over the Pacific, while a weak monsoon season is associated with weak trade winds.

The major objectives of the present work are 1) to reexamine the onset of the Asian summer monsoon in relation to the large-scale land–sea thermal contrast and the processes contributing to the contrast; and 2) to compare strong and weak Asian summer monsoon years in terms of the land–sea thermal contrast, and its contributing factors such as SST, cumulus convection, and distribution of heat sources.

## 2. Data and analysis procedures

To accomplish the objectives of this work, a 14-yr (1979–1992) dataset in the domain 50°S–50°N; 0°–

360° (see Fig. 1) is used. The dataset includes the following:

1) The horizontal wind components $u$ and $v$, and temperature $T$ and mixing ratio $q$ from the European Center for Medium-Range Weather Forecasts (ECMWF) FGGE Level III-b analyses (0000 and 1200 UTC) for 1979 at 14 standard pressure levels and regridded on a 2.5° × 2.5° lat–long mesh. In the FGGE data, $u$ and $v$ are not initialized, but $T$ and $q$ are initialized.

2) The $u$, $v$, $T$, and $q$ from the ECMWF/World Meteorological Organization (WMO) global analyses (0000 and 1200 UTC) from 1980 to 1984 at seven standard pressure levels on a 2.5° × 2.5° grid. All field variables are initialized.

3) The $u$, $v$, $T$, and $q$ from the ECMWF/Tropical Oceans and Global Atmosphere (TOGA) global analyses (0000 and 1200 UTC) from 1985 to 1992 at 14 standard pressure levels on a 2.5° × 2.5° grid. In this dataset, all variables are uninitialized. In this work we used this subset for the computation of $\omega$, $Q_1$, and $Q_2$ as given below.

4) Daily outgoing longwave radiation (OLR) on a 2.5° × 2.5° grid from 1979 to 1992.

5) National Meteorological Center (NMC) Climate Analysis Center (CAC) monthly sea surface temperature (SST) analyses on a 2° × 2° grid from 1979 to 1992.

In addition, the apparent heat source $Q_1$ and the apparent moisture sink $Q_2$ (e.g., Yanai et al. 1973, 1992) are computed from

$$Q_1 = C_p \left(\frac{p}{p_0}\right)^{\kappa} \left(\frac{\partial \theta}{\partial t} + \mathbf{v}\cdot\nabla\theta + \omega\frac{\partial \theta}{\partial p}\right), \quad (1)$$

$$Q_2 = -L\left(\frac{\partial q}{\partial t} + \mathbf{v}\cdot\nabla q + \omega\frac{\partial q}{\partial p}\right). \quad (2)$$

In (1) and (2), $\theta$ is the potential temperature, $\mathbf{v}$ the horizontal velocity, $\omega$ the vertical $p$ velocity, $p$ the pressure. Here $\kappa = R/C_p$, $R$ and $C_p$ are the gas constant and the specific heat at constant pressure of dry air, $p_0$ = 1000 hPa, and $L$ the latent heat of condensation; $\nabla$ is the isobaric gradient operator.

It is important to note that the accuracy of $Q_1$ and $Q_2$ estimates crucially depends on the accuracy of $\omega$, which is a highly scheme dependent quantity. In this work $\omega$ is recomputed from the horizontal divergence by vertically integrating the continuity equation with certain constraints (appendix A). Here $Q_1$ and $Q_2$ are calculated for the layer between the ground surface and the first standard pressure level above the surface, and for each successive layer between the standard pressure levels. The advection terms in (1) and (2) are evaluated at every observation time, and the local time change terms are evaluated using the centered time difference of $\theta$ and $q$ over 24 h.

As shown by Yanai et al. (1973), the vertical integration of (1) and (2) from the tropopause pressure $p_T$ to the surface pressure $p_s$ gives

$$\langle Q_1 \rangle = \langle Q_R \rangle + LP + S, \quad (3)$$

$$\langle Q_2 \rangle = L(P - E), \quad (4)$$

where

$$\langle\ \rangle = \frac{1}{g}\int_{p_T}^{p_s} (\ )\,dp. \quad (5)$$

Here $P$, $S$, and $E$ are the precipitation rate, the sensible heat flux, and the evaporation rate, respectively, per unit area at the surface. Because of these relations, comparison between the horizontal distributions of $\langle Q_1 \rangle$ and $\langle Q_2 \rangle$ will yield information on the nature of heating processes (e.g., Luo and Yanai 1984; Yanai et al. 1992).

As discussed by several authors (e.g., Trenberth and Olson 1988; Hoskins et al. 1989; Schaack and Johnson 1994), the continuity of the ECMWF analyses in the dataset was impacted by the changes routinely made to assimilation systems for the purpose of improving numerical weather prediction. Thus, derived fields such as $\omega$, $Q_1$, and $Q_2$ may be sensitive to some changes introduced in the assimilation system. In this study $Q_1$ and $Q_2$ are calculated only from 1985 to 1992 using the ECMWF/TOGA data, because the data quality during this period appears to be relatively uniform and has a relatively high vertical resolution. Even during this period, some changes in the ECMWF analysis/forecast scheme were made (e.g., Trenberth 1992). As stated by Schaack and Johnson (1994), the impact of these changes on the analyses is difficult to estimate. However, inspection of time series of vertically integrated $\langle Q_1 \rangle$ and $\langle Q_2 \rangle$ in selected regions (not shown) finds no evidence of discontinuities at major changes of the assimilation scheme (e.g., May 1985, May 1989) shown in Table 1 of Trenberth (1992).

## 3. Climatology of the summer monsoon circulation

In this section, wind, temperature, SST, and OLR flux are averaged over the 14-yr period from 1979 to 1992. Here $Q_1$ and $Q_2$ are averaged over the 8-yr period from 1985 to 1992.

The summer (June, July, and August) mean flow patterns at 850 and 200 hPa are shown in Fig. 2. At 850 hPa the prominent wind systems are the cross-equatorial flow along the east coast of Africa and the easterly trade winds in the tropical Pacific. Under the effect of the Coriolis force, the cross-equatorial flow becomes the southwest monsoon in South Asia and meets with the trade winds in the western Pacific. There is a high pressure system on both sides of the equator over the Pacific and Atlantic Oceans. Over the Indian sector, however, the symmetry is broken by the Asian land mass and a high pressure system forms only over

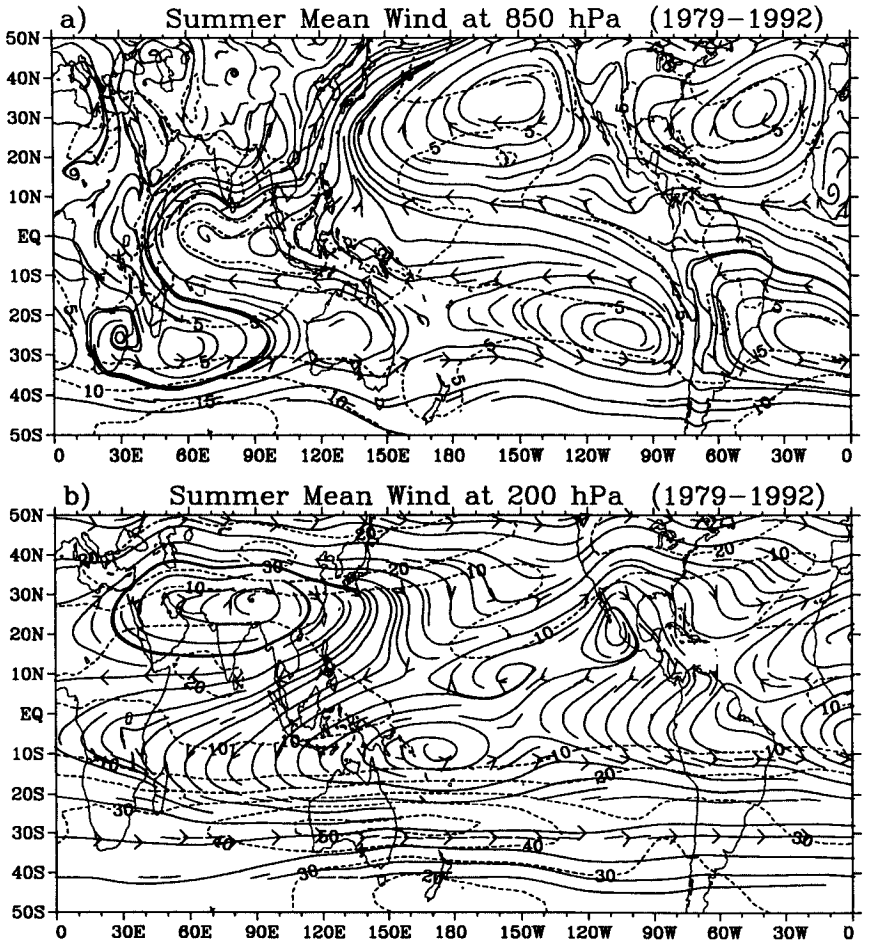


FIG. 2. The summer (June–August) mean streamlines and isotachs (m $s^{-1}$) at (a) 850 hPa and (b) 200 hPa, averaged over 14 years (1979–1992).

the south Indian Ocean. At 200 hPa, the most outstanding features are the huge anticyclonic circulation (the so-called Tibetan High) centered over the southern edge of the Tibetan Plateau, and the cross-equatorial flow from the Northern Hemisphere to the Southern Hemisphere along the eastern and southern periphery of the Tibetan High. Compared to the Tibetan High, the anticyclonic circulation over Mexico is much weaker and smaller. Between the Tibetan and Mexican anticyclones is a deep trough over the mid-Pacific Ocean, resulting in the southwesterly flow to the south of the trough. The circulation over high latitudes of the Southern Hemisphere is more zonally oriented.

Figure 3 shows the horizontal distribution of the 200–500-hPa layer mean temperature for summer. A huge warm air mass is centered on South Asia with the maximum temperature ($\geq -22$°C) over the southern Tibetan Plateau, resulting in strong temperature gradients in both the north–south and east–west directions. A warm temperature ridge exists over the North American continent. A deep temperature trough stretches from the west coast of North America to the central Pacific. A temperature trough is also observed over the Atlantic Ocean. The upper-tropospheric flow pattern (Fig. 2b) clearly reflects the thermal contrast between continents and oceans.

The summer mean SST distributions are shown in Fig. 4a. Warm SSTs ($\geq$28°C) are over the tropical western Pacific, South China Sea, and most part of the North Indian Ocean where the southwesterly monsoon prevails. The warm SSTs are also observed along the intertropical convergence zone (ITCZ) in the eastern Pacific and in the Gulf of Mexico. The cold SST ($\leq$26°C) originates along the coast of South America and a cold tongue extends westward to the central Pacific. Figure 4b shows the summer mean distributions of the OLR flux. The regions with the OLR values less than 240 W $m^{-2}$ are shaded. In the Tropics, the OLR flux less than 240 W $m^{-2}$ indicates the presence of deep cumulus convection. However, in the high latitude and high altitude regions, low OLR values may indicate the cold ground surface temperature. The organized deep

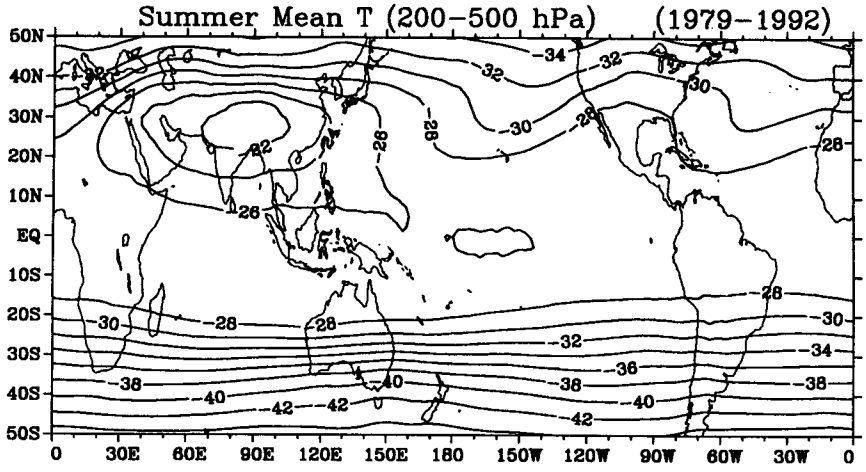


FIG. 3. The mean upper-tropospheric (200–500 hPa) temperature (°C) for summer, averaged over 14 years (1979–1992).

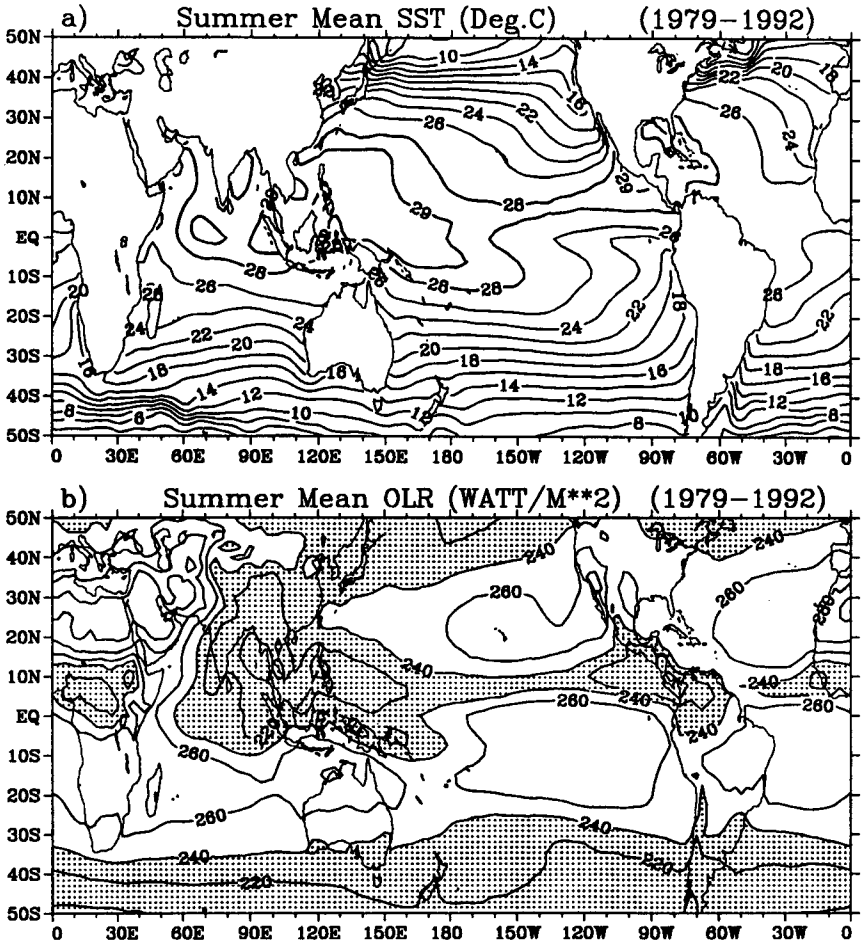


FIG. 4. The summer mean (a) SST (°C) and (b) OLR flux (W $m^{-2}$), averaged over 14 years (1979–1992). The shaded regions indicate the OLR flux less than 240 W $m^{-2}$.

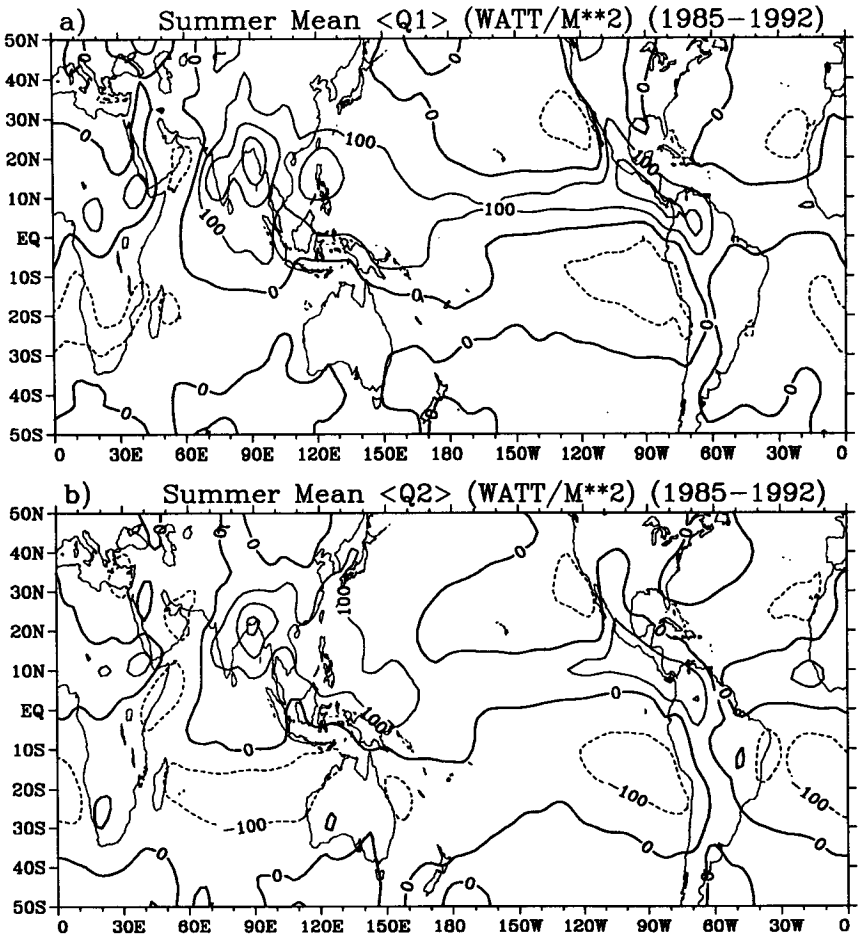


FIG. 5. (a) The vertically integrated heat source $\langle Q_1 \rangle$, and (b) the vertically integrated moisture sink $\langle Q_2 \rangle$ for summer, averaged over 8 years (1985–1992). Contour interval is 100 W m$^{-2}$.

convection (thus implied heavy precipitation) is mainly confined in the Asian southwesterly monsoon region and the western Pacific warm pool, with the eastward extension to the ITCZ in the eastern Pacific and Central America. Comparison with the SST (Fig. 4a) shows that the organized deep convection in the tropical oceanic region is well associated with the warm SSTs ($\geq$28°C). Deep convection is also found over Central Africa. The OLR values are greater than 260 W m$^{-2}$ in the South Indian Ocean, the northeastern and southeastern Pacific, and the North and South Atlantic, indicating cloud-free regions under large-scale subsidence. Very large OLR values ($\geq$300 W m$^{-2}$) are found over dry land areas including the Sahara Desert, the Saudi Arabian Desert, and the Iran–Afghanistan region, reflecting high ground surface temperature there.

The summer mean horizontal distributions of the vertically integrated heat source $\langle Q_1 \rangle$ and moisture sink $\langle Q_2 \rangle$ are shown in Fig. 5. Intense heating ($\geq$100 W m$^{-2}$) is located in the Asian monsoon region with the maximum heating over the Bay of Bengal coast ($\sim$300 W m$^{-2}$) and in the western Pacific Ocean, and extends further to the Pacific ITCZ and Central America. Intense cooling ($\leq -100$ W m$^{-2}$) is over the eastern parts of the North and South Pacific and Atlantic Oceans, the western Arabian Sea and South Africa. Over the tropical oceanic regions, large positive values ($\geq$100 W m$^{-2}$) of $\langle Q_1 \rangle$ are accompanied by similar values of $\langle Q_2 \rangle$ and small OLR values ($\leq$240 W m$^{-2}$) (Fig. 4b), indicating that heating is mostly contributed by the release of latent heat of condensation associated with deep cumulus convection. On the other hand, large negative values ($\leq -100$ W m$^{-2}$) of $\langle Q_1 \rangle$ over subtropical oceans are accompanied by $\langle Q_2 \rangle$ of similar magnitude and large OLR values ($\geq$260 W m$^{-2}$), suggesting the dominance of radiative cooling and moistening due to evaporation from the sea surface. We note, however, that sensible heat is important over the Tibetan Plateau region as suggested by significant values of $\langle Q_1 \rangle$ (100–200 W m$^{-2}$) accompanied by smaller values of $\langle Q_2 \rangle$ (50–100 W m$^{-2}$).

## 4. Evolution of the Asian summer monsoon

The onset of the Asian summer monsoon is marked by the establishment of a southwesterly flow at lower levels and an easterly flow at upper levels over the North Indian Ocean and Southeast Asia. In Fig. 6a we present the longitude-time section at 15°N showing the mean annual cycle of the intensity of southwesterlies at 850 hPa. The major southwesterlies at this level are found only over longitudes covering from the Arabian Sea to the South China Sea (between 50° and 120°E). A weak southwesterly flow ($\sim$1 m s$^{-1}$) starts near 100°E in late January. The southwesterlies of moderate intensity ($\sim$5 m s$^{-1}$) first appear in the Bay of Bengal and Southeast Asia (between 80°E and 110°E) in mid-May, and then extend to the Arabian Sea (between 50°E and 70°E) in early June. In summer there are two major branches of the southwesterlies, corresponding to the Southeast Asian summer monsoon and the Indian summer monsoon, respectively (He et al. 1987). Weak southwesterlies ($\sim$1 m s$^{-1}$) are also observed in North Africa (between 20°E and 40°E) in summer. The southwesterlies ($\geq$5 m s$^{-1}$) disappear altogether by the end of September.

The longitude–time section at 15°N of the mean zonal wind velocity at 200 hPa is shown in Fig. 6b. Intense easterlies ($\leq -10$ m s$^{-1}$) occur between 0° and 120°E during the summer months. The zonal wind in this sector rapidly changes from westerlies to easterlies in the middle of May and attains the maximum intensity in July and August and then gradually changes from easterly back to westerly in fall. The transition from westerlies to easterlies occurs first in Southeast Asia (near 100°E). Weak easterlies are also observed over the tropical eastern Pacific (between 140°W and 90°W), which are associated with the Mexican High.

The time evolution of the monsoon circulation described above is linked to the changes in the tropospheric temperature. Figure 7a shows the longitude–time section of the anomaly of the upper-tropospheric (200–500 hPa) temperature from the whole domain and annual mean. This section is taken along the 30°N lat, which cuts through the temperature maximum over the Tibetan Plateau (see Fig. 3). Temperature anomalies begin to change from negative to positive in April near 90°–100°E. The temperature increases over Eurasia during summer are much larger than those over North America. The maximum temperature anomaly ($\geq$10 K) occurs in the region of the Tibetan Plateau (between 60°E and 105°E). In contrast, there is no appreciable change in the upper-tropospheric temperature along 5°N (mostly over oceans) (Fig. 7b).

Figure 8a shows the longitude–time section of the difference of the mean upper-tropospheric (200–500 hPa) temperature between 5° and 30°N. In the shaded areas of this figure, the mean meridional temperature gradient is positive. The reversal of the meridional temperature gradient occurs first on the southside of the

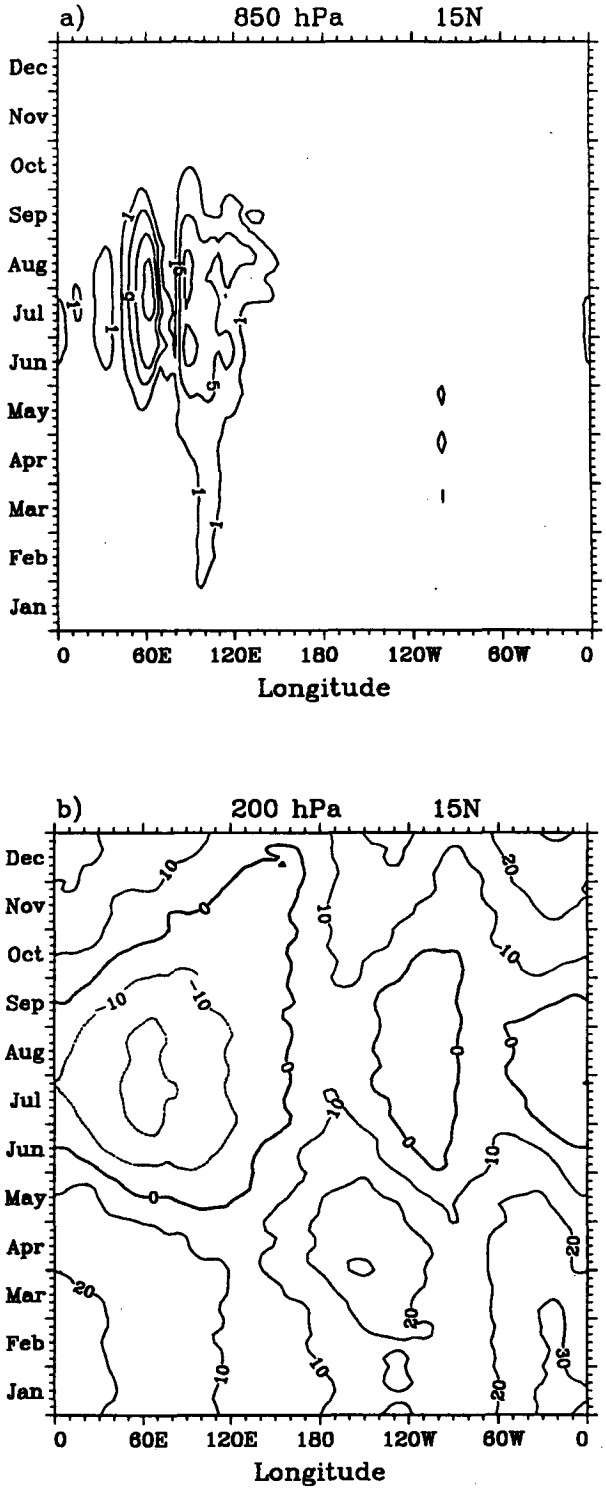


FIG. 6. Longitude–time sections at 15°N showing the annual cycle of (a) the 5-day mean intensity (m s$^{-1}$) of the southwesterlies ($u > 0, v > 0$) at 850 hPa, and (b) the 5-day mean zonal wind component (m s$^{-1}$) at 200 hPa, averaged over 14 years (1979–1992).

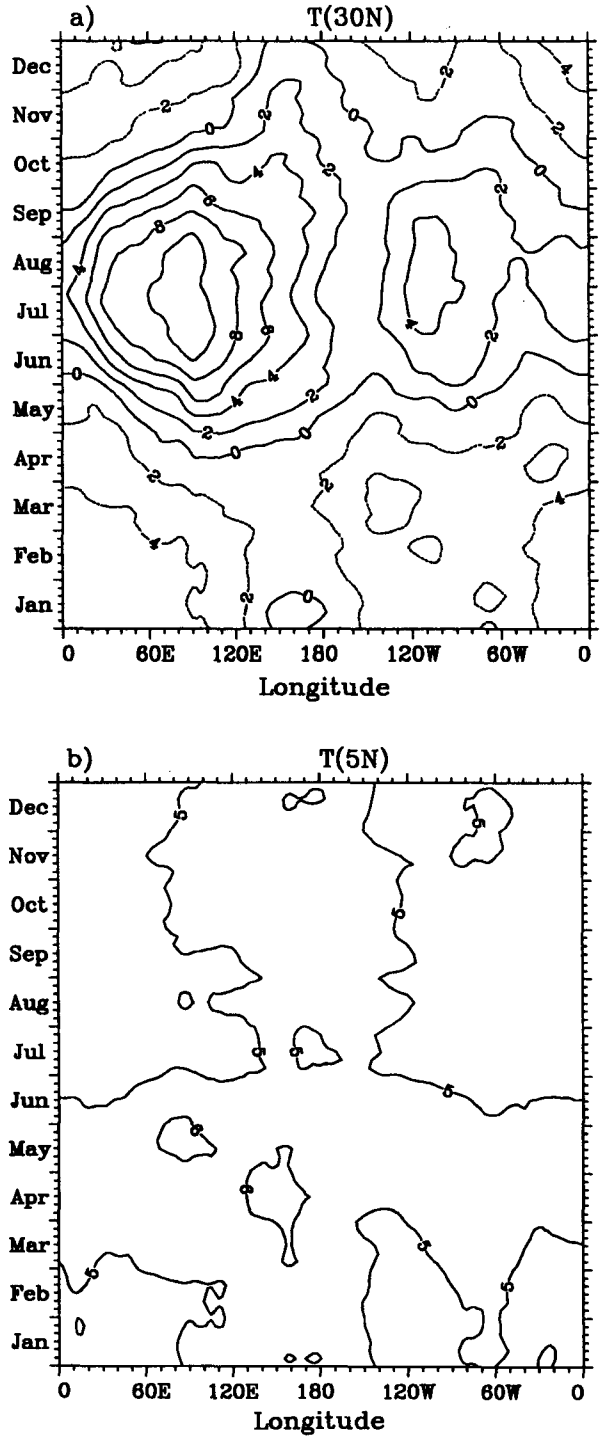


FIG. 7. Longitude–time sections showing the annual cycle of the 5-day mean anomaly of the upper-tropospheric (200–500 hPa) temperature (°C) from the annual and whole domain average at (a) 32.5°N and (b) 15°N, averaged over 14 years (1979–1992).

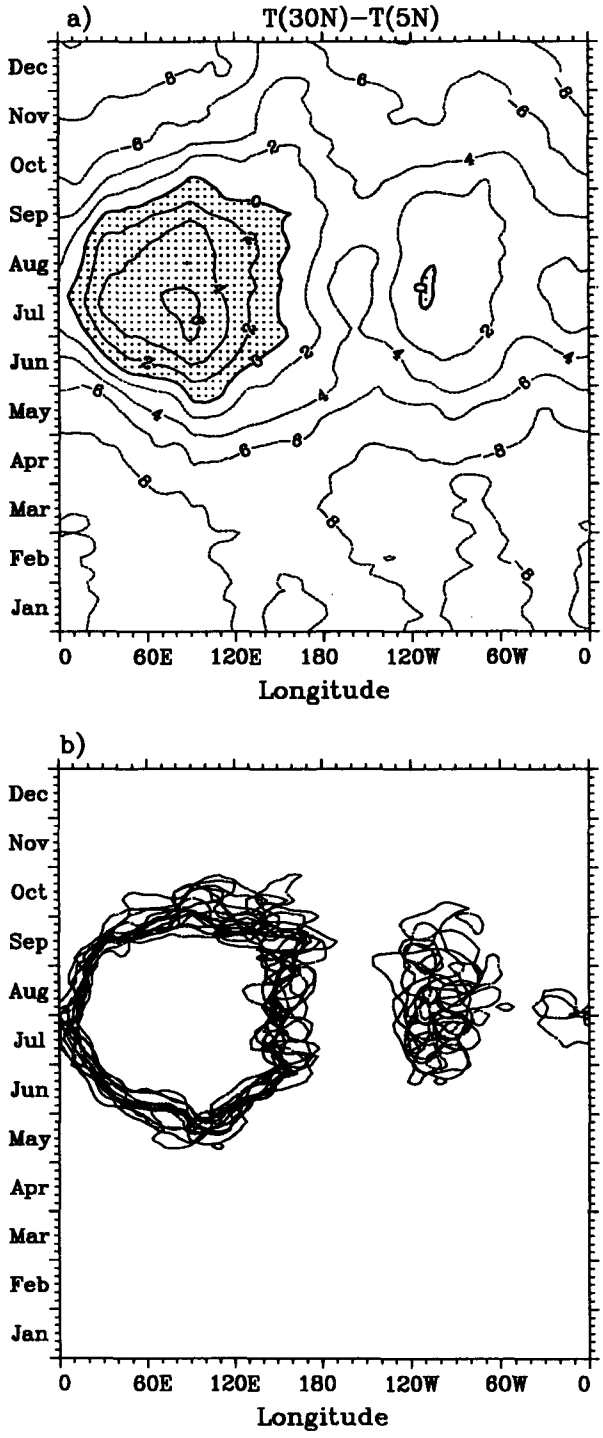


FIG. 8. Longitude–time sections showing (a) the 5-day mean upper-tropospheric (200–500 hP) temperature (°C) at 30°N minus that at 5°N (areas of positive values are shaded); and (b) contours of "zero" temperature difference for individual years.

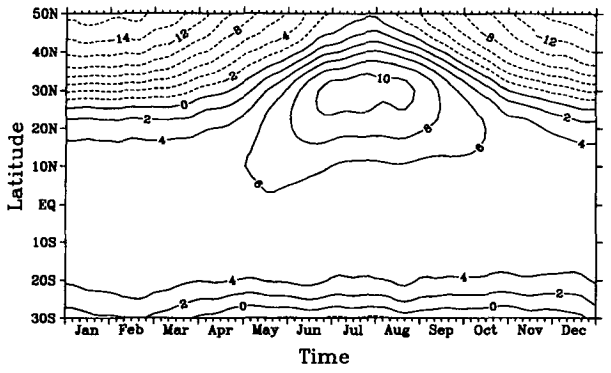


FIG. 9. Latitude–time section showing the 14-yr (1979–1992) mean annual cycle of the 5-day mean anomaly of the upper-tropospheric (200–500 hPa) temperature (°C) from the annual and domain mean, averaged between 70° and 100°E.

Tibetan Plateau (near 90°–100°E) and then expands over a large area extending from Africa to the western Pacific. The temperature difference attains the maximum values (>6 K) in July and becomes negative in September to October. The dominant role played by the temperature increases over land areas centered on the Tibetan Plateau in this reversal is evident from Figs. 7a,b and 8a. To see the year-to-year variation of the timing and longitudinal extent of the reversal of meridional temperature gradient, contours of "zero" gradient for years (1979–1992) are superimposed upon each other in Fig. 8b. The beginning and ending of the reversal can vary on the order of one month. It is noted that the eastern extension of the reversal vary significantly year by year.

The annual cycle of the upper-tropospheric (200–500 hPa) temperature is clearly seen also in the latitude–time section of its anomalies averaged between 70° and 100°E (Fig. 9). Warm anomaly (>6 K) appears from May to October and its center is located on the southern Tibetan Plateau (30°N) in summer. Note that large seasonal temperature changes occur only to the north of 10°N, and there is no appreciable change over the Indian Ocean south of 10°N.

Figures 10a–c show the latitude–time sections of the mean $\langle Q_1 \rangle$, $\langle Q_2 \rangle$, and OLR flux averaged between 70° and 100°E, respectively. The equatorial Indian Ocean is a heat source throughout the year. However, large asymmetry exists in the location and magnitude of heat sources between the hemispheres. In winter a heat sink exists to the north of 10°N. In February to March the Tibetan Plateau region (25°–50°N) becomes a heat source. Note that this heat source is separated from the more intense heat source over the equatorial Indian Ocean by the heat sink over the Indian subcontinent (10°–25°N). In spring, the heating over land is enhanced and extended southward. At about the same time the oceanic heat source starts to migrate northward and begins to merge with the heat source over the land. The heating between 10° and 30°N is rapidly increased in late May, when the meridional temperature gradient south of the Plateau is reversed (see Fig. 8a) and the Asian summer monsoon is commenced (see Fig. 6a). After the onset of monsoon, the heating maximum reaches about 20°N. Comparisons of $\langle Q_1 \rangle$ with $\langle Q_2 \rangle$ (Fig. 10b) and OLR flux (Fig. 10c) shows that the heat source over the ocean is mostly contributed by the release of latent heat of condensation. Figure 10c shows the northward advance of the rain belt (OLR $\leq$ 240 W m$^{-2}$) from the equatorial area in winter to the foothills of Himalayas in summer as previously discussed by Krishnamurti (1985), Murakami and Nakazawa (1985), and Murakami and Matsumoto (1994).

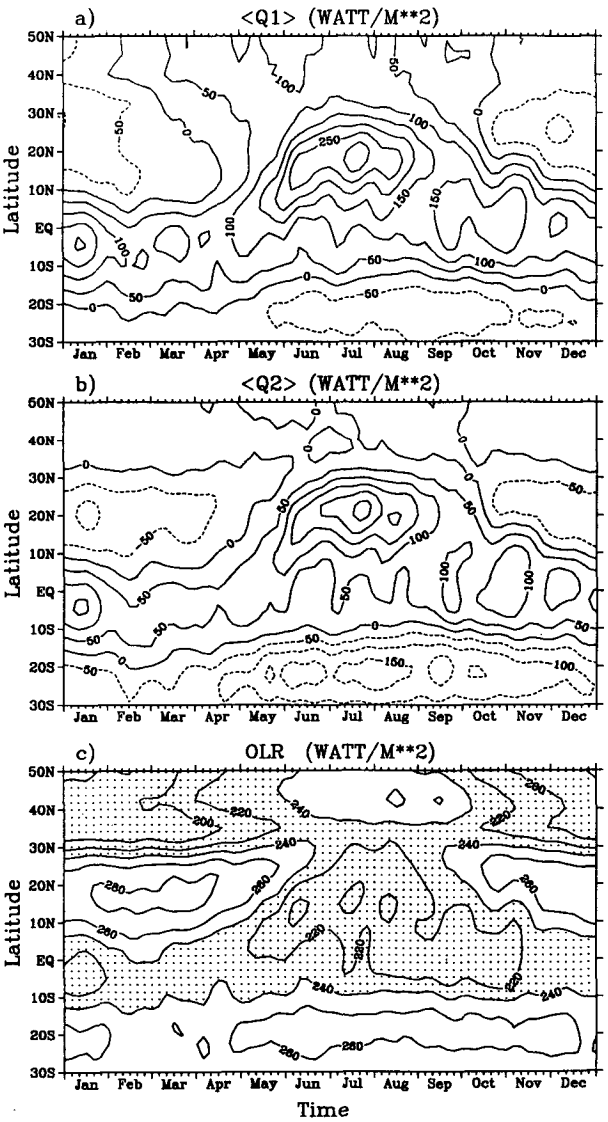


FIG. 10. Latitude–time sections showing the 8-yr (1985–1992) mean annual cycle of the 5-day mean (a) $\langle Q_1 \rangle$, (b) $\langle Q_2 \rangle$ and (c) OLR flux, averaged between 70°E and 100°E (units: W m$^{-2}$).

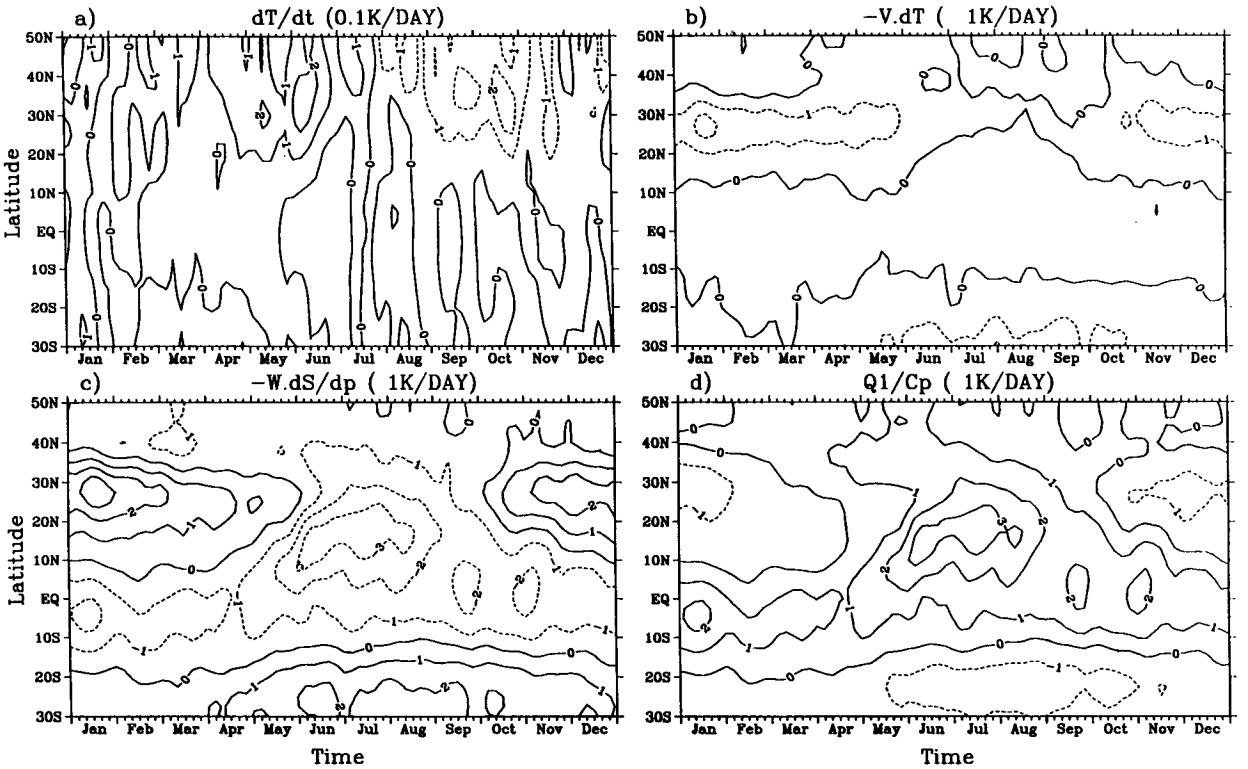


FIG. 11. Latitude–time sections showing the analysis of the time change of the 200–500-layer mean temperature averaged between 70°E and 100°E. (a) The local time change (0.1 K day$^{-1}$), (b) the horizontal advection (K day$^{-1}$), (c) the vertical advection (K day$^{-1}$), and (d) the diabatic heating (K day$^{-1}$) [see Eq. (6)].

When we compare the migration of heat sources (Fig. 10) with the actual time change of upper-tropospheric temperature (Fig. 9), it is evident that they do not resemble each other. To examine the mechanism that generates the warm center at 30°N, we analyze each term of the thermodynamic energy equation

$$\frac{\partial \hat{T}}{\partial t} = -\mathbf{v}\cdot\nabla T - \left(\frac{p}{p_0}\right)^{\kappa}\omega\frac{\partial\theta}{\partial p} + \frac{Q_1}{C_p}, \qquad (6)$$

averaged over the 200–500-hPa layer.

Figure 11 shows the latitude–time sections of the four terms of Eq. (6) averaged between 70° and 100°E. Significant changes of the mean upper-tropospheric temperature (0.1–0.2 K day$^{-1}$) occur only at latitudes north of 20°N (Fig. 11a). The cooling due to cold horizontal advection (approximately −1 K day$^{-1}$) is seen between 20° and 30°N except in summer months (Fig. 11b). The most remarkable feature in Fig. 11 is that the adiabatic cooling (Fig. 11c) nearly compensates the heat source term (Fig. 11d). An exception is the heat source (~1 K day$^{-1}$) appearing from April to July to the north of 30°N (Fig. 11d) where significant temperature increase is observed (Fig. 11a). This analysis illustrates that despite its large values the released latent heat of condensation with the migrating rain belt does not directly affect the upper-tropospheric temperature over the Indian Ocean. Instead, sensible heating in May–June over land surface is the primary cause of warming over the Tibetan Plateau. Additional detailed analyses of time series of temperature, $\langle Q_1\rangle$ and $\langle Q_2\rangle$ over the Plateau (not shown) reveal that the heat released by condensation also contributes to the heating of the eastern Plateau after the monsoon onset, as shown by previous studies for 1979 (Nitta 1983; Luo and Yanai 1984; He et al. 1987; Yanai et al. 1992; Yanai and Li 1994a).

## 5. Strong versus weak Asian summer monsoon

To discuss the interannual variability of the Asian monsoon, a measure of the monsoon intensity must be defined. Three independent data can be used to define the intensity of the monsoon. These are the intensity of monsoonal circulation, satellite-measured OLR field, and precipitation amounts over a representative area. Following Webster and Yang (1992), we choose the vertical shear of zonal wind between 850 and 200 hPa,

$$S_1 = u(850\text{ hPa}) - u(200\text{ hPa}), \qquad (7)$$

averaged over summer and the region 0°–20°N, 40°–110°E (see Fig. 1) as the index of intensity of broad-

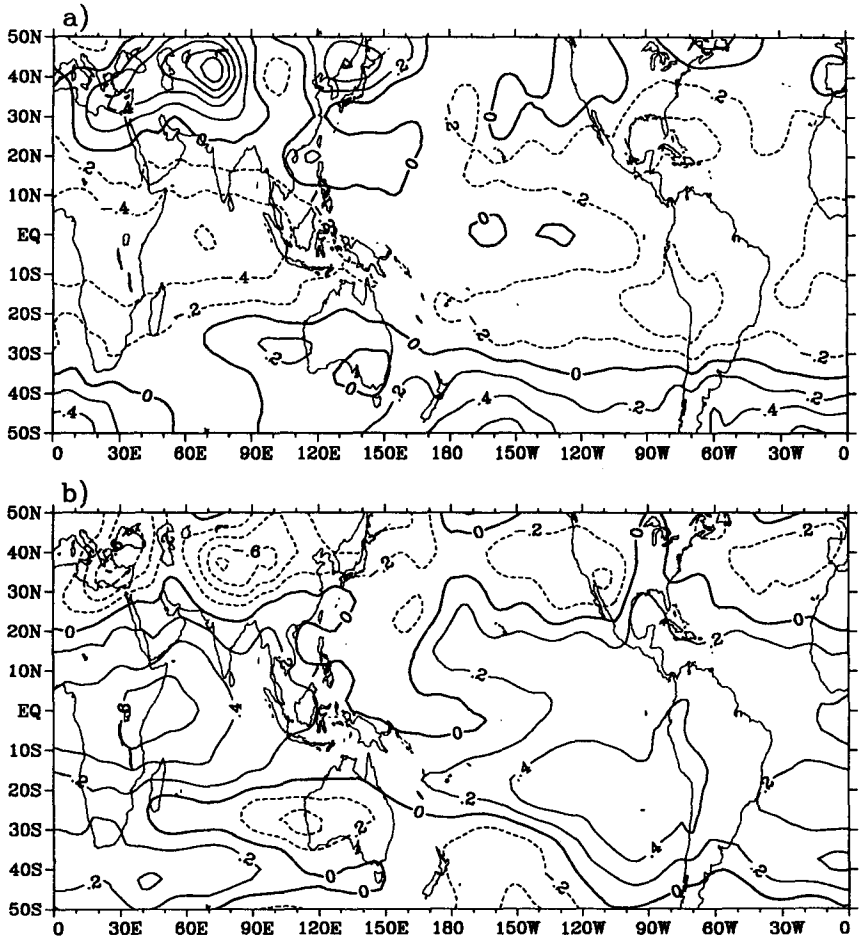


FIG. 12. The summer mean anomalies of the upper-tropospheric (200–500 hPa) temperature for (a) the strong monsoon years and (b) the weak monsoon years. Contour interval is 0.2°C.

scale Asian summer monsoon. Comparison of this index with other tested indices are given in appendix B.

Using the time series of the deviation of the summer (June, July, August) mean monsoon index from the 14-summer (1979–1992) mean (Fig. B1), we choose 1.5 m $s^{-1}$ as a threshold value. If the monsoon index anomaly of a particular year is larger than 1.5 m $s^{-1}$, that year is classified as a strong monsoon year. If the monsoon index anomaly of a particular year is less than $-1.5$ m $s^{-1}$, that year is categorized as a weak monsoon year. Using this classification, four strong monsoon years and four weak monsoon years are identified. Strong monsoon years are 1984, 1985, 1986, and 1990. Weak monsoon years are 1979, 1982, 1983, and 1987. The anomalies of variables described below are from the 14-yr (1979–1992) mean values unless stated otherwise. Webster and Yang (1992) made composite studies of the zonal wind and OLR fields for the strong and weak monsoon years using the data from 1979 to 1987. They showed that the Pacific trade wind and the east–west circulation were intensified during the strong monsoon years, while these were weak during the weak monsoon years. These results were confirmed with the extended dataset (see Li 1994 for details). Here, we extend their study to other variables such as the tropospheric temperature, SST, and diabatic heating.

Figures 12a and 12b illustrate the summer mean anomalies of the 200–500 hPa layer mean temperature averaged for the strong and weak monsoon years, respectively. In the strong monsoon years (Fig. 12a), large positive temperature anomalies cover most of the central and northeastern Asia. Southern Hemisphere midlatitudes are also the regions of positive temperature anomalies. Negative temperature anomalies occupy the tropical belt including large areas of the Indian, eastern Pacific, and Atlantic Oceans and the African and American continents. The distribution of temperature anomalies shows enhanced meridional as well as longitudal land–sea temperature contrasts. The weak-monsoon-year temperature anomalies (Fig. 12b) are in complete contrast to those of the strong-monsoon-year. Major negative temperature anomalies are

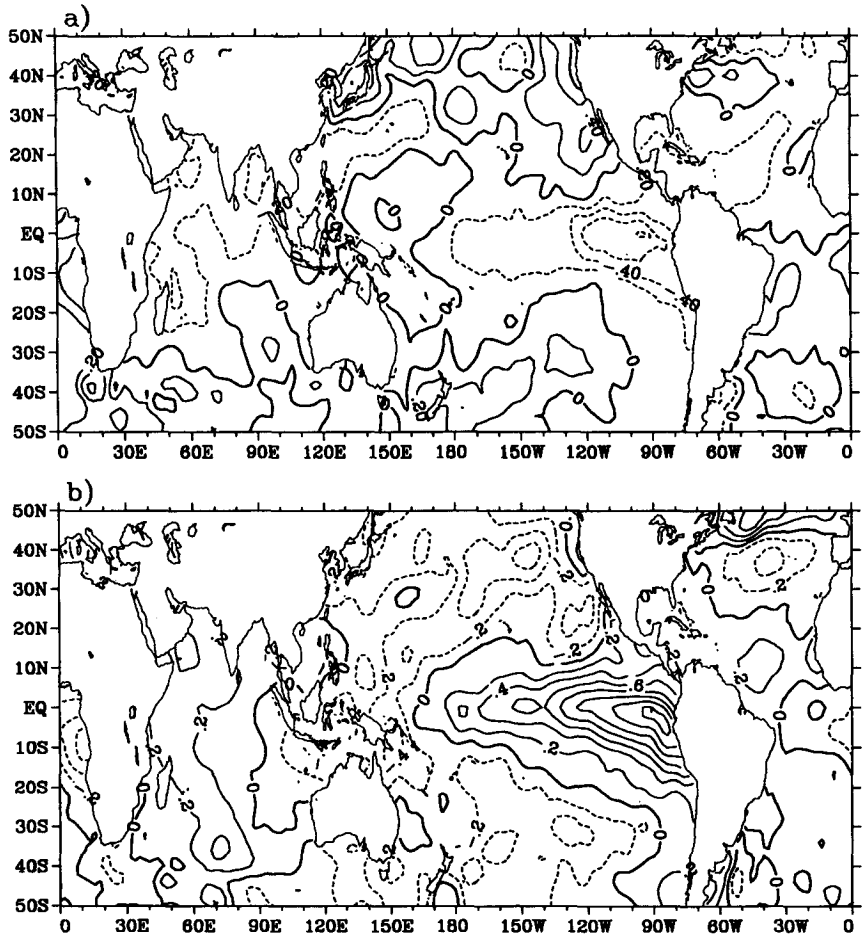


FIG. 13. The summer mean anomalies of SST for (a) the strong monsoon years and (b) the weak monsoon years. Contour interval is 0.2°C.

over the regions north of 20°N with two minimum centers located over the Eurasian land mass. Negative anomalies also exist in the Southern Hemisphere, that is, over the South Indian Ocean–Australia region and the central South Pacific. Large positive anomalies are located over the tropical Indian Ocean–Africa region and the eastern Pacific. Such distributions of temperature anomalies indicate reduced meridional as well as longitudinal temperature contrasts.

Figure 13a shows the summer SST anomalies averaged for the strong monsoon years. A tongue of negative SST anomalies extends from the west coast of South America westward to the equatorial central Pacific, forming a SST distribution similar to that of a cold event or La Niña. Negative SST anomalies are also found over the oceans adjacent to South and East Asia, that is, the Indian Ocean, the South and East China Seas, and part of the western Pacific. Positive SST anomalies are located in the equatorial western Pacific, the North Pacific, and the Southern Hemisphere midlatitudes. The summer SST anomalies of the weak monsoon years (Fig. 13b) are in sharp contrast to those of the strong monsoon years. Large positive SST anomalies are along the equator over the central and eastern Pacific Ocean, forming an SST distribution similar to that of a warm event or El Niño. Weak positive SST anomalies are also found over the western Indian Ocean and the oceans adjacent to Southeast Asia. Krishnamurti et al. (1989) described similar warm SST anomaly distributions during summer months of 1987. Negative SST anomalies extend from the equatorial western Pacific to the North and South Pacific Oceans of middle latitudes.

In the strong monsoon years the OLR flux shows negative anomalies over the Indian subcontinent, Indonesia, the South China Sea, and the western North Pacific (Fig. 14a). Positive OLR anomalies exist along the equator from the central Pacific eastward to the west coast of Central America. The distribution of OLR anomalies in the strong monsoon years suggests that cumulus convection is strong in the Asian monsoon region and the western Pacific but weak in the equa-

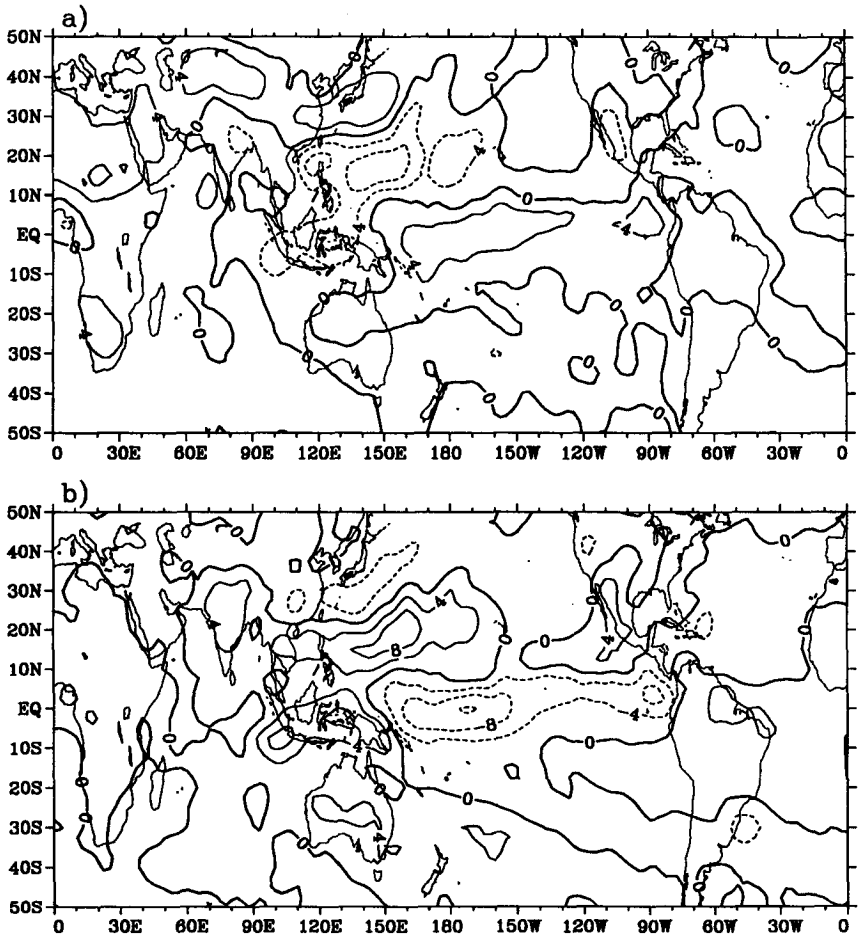


FIG. 14. The summer mean OLR anomalies for (a) the strong monsoon years and (b) the weak monsoon years. Contour interval is 4 W $m^{-2}$.

torial central and eastern Pacific. In the weak monsoon years the OLR anomalies are in complete contrast to those in the strong monsoon years (Fig. 14b). Positive OLR anomalies are found in the regions extending from the Indian Ocean and the Indian subcontinent to Indonesia, Indochina, and the western North Pacific Ocean. A belt of negative OLR anomalies extends along the equator from the central Pacific to the west coast of Central America. Krishnamurti et al. (1989) showed a similar distribution of OLR anomalies during summer 1987. Comparing with the distributions of the SST anomalies (Fig. 13), we find that the OLR and SST anomalies are negatively correlated in the equatorial central and eastern Pacific.

The calculations of heat sources and moisture sinks are made only for 8 yr from 1985 to 1992. Within these 8 years, there are three strong monsoon years (1985, 1986, and 1990). However, only the year 1987 is a weak monsoon year in this period. The year 1987 was a year of drought in India and El Niño–related warm SST anomalies were observed in the eastern and central equatorial Pacific (e.g., Krishnamurt et al. 1989). In Figs. 15 and 16 we show anomalies of heat sources and OLR in 1985 and 1987 for comparison. In summer 1985, the heating is enhanced over the Arabian Sea, the Bay of Bengal, Indonesia, and the western Pacific near the Philippines, while the heating over the equatorial Indian Ocean and the equatorial central and eastern Pacific is reduced (Fig. 15a). These are consistent with the OLR anomalies for the same year (Fig. 15b). In summer 1987, the heating over South Asia is significantly weakened, while heating over the equatorial central Pacific is remarkably enhanced (Fig. 16a). The enhanced heating over the equatorial Pacific is supported by the large negative OLR anomalies in this region (Fig. 16b).

## 6. Summary and discussion

We have described the onset and interannual variability of the Asian summer monsoon in terms of the large-scale land–sea thermal contrast and related pro-

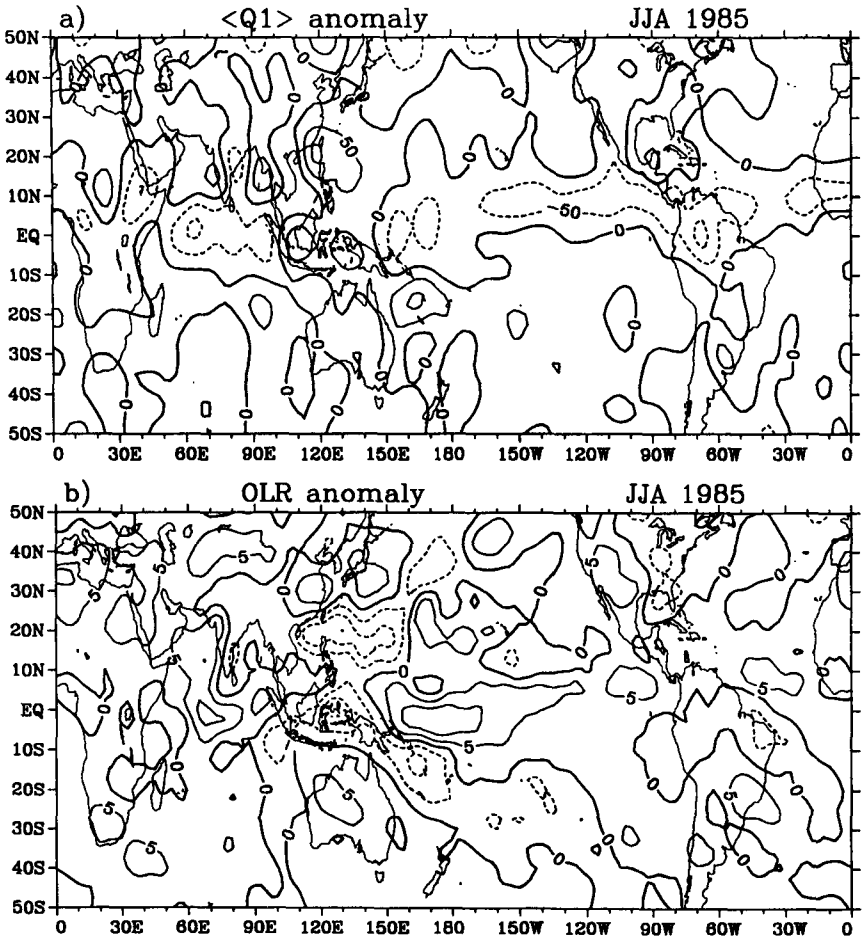


FIG. 15. The anomalies of (a) the vertically integrated heat source $\langle Q_1 \rangle$ and (b) OLR flux from the 8-yr (1985–1992) mean for summer 1985 (units: W $m^{-2}$).

cesses such as the SST, cumulus convection, and heat source distributions. The major findings of this work are summarized in the following with suggestions for further research.

1) The deep lower-tropospheric southwesterly flow characterizing the Asian summer monsoon is a uniquely conspicuous phenomenon in the global circulation, which exists only on the south side of the heated land centered around the Tibetan Plateau. Its onset is concurrent with the reversal of meridional temperature gradient south of the Tibetan Plateau. The reversal is chiefly the result of large temperature increase over the Plateau region with no appreciable temperature change over the Indian Ocean. These confirm Flohn's (1957, 1960) classical hypothesis and the more recent analyses of He et al. (1987) and Yanai et al. (1992) for the FGGE year.

2) In spring the Tibetan Plateau is a heat source that is distinctly separate from the more intense heat source associated with the rain belt in the equatorial Indian Ocean. The Tibetan heat source is mainly contributed by sensible heating from the ground surface, while the oceanic heat source is due to the release of latent heat of condensation. It is noted that the heat of condensation, despite its intensity, does not cause appreciable temperature changes over the Indian Ocean because of compensating effect of adiabatic cooling. It is the sensible heating over land in spring that leads to the eventual reversal of meridional gradient of temperature. These tend to confirm the results of previous studies of heating processes over the Tibetan Plateau and the surrounding regions (Luo and Yanai 1984; He et al. 1987; Yanai et al. 1992; Yanai and Li 1994a) and further demonstrate the thermal influence of the Tibetan Plateau as a dominant factor driving the planetary-scale monsoon system.

3) Our study also confirmed the associations of strong and weak monsoon years with anomalous SST and OLR distributions (e.g., Meehl 1987; Krishnamurti et al. 1989; Webster and Yang 1992). Many studies have shown that the changes in the atmospheric/oce-

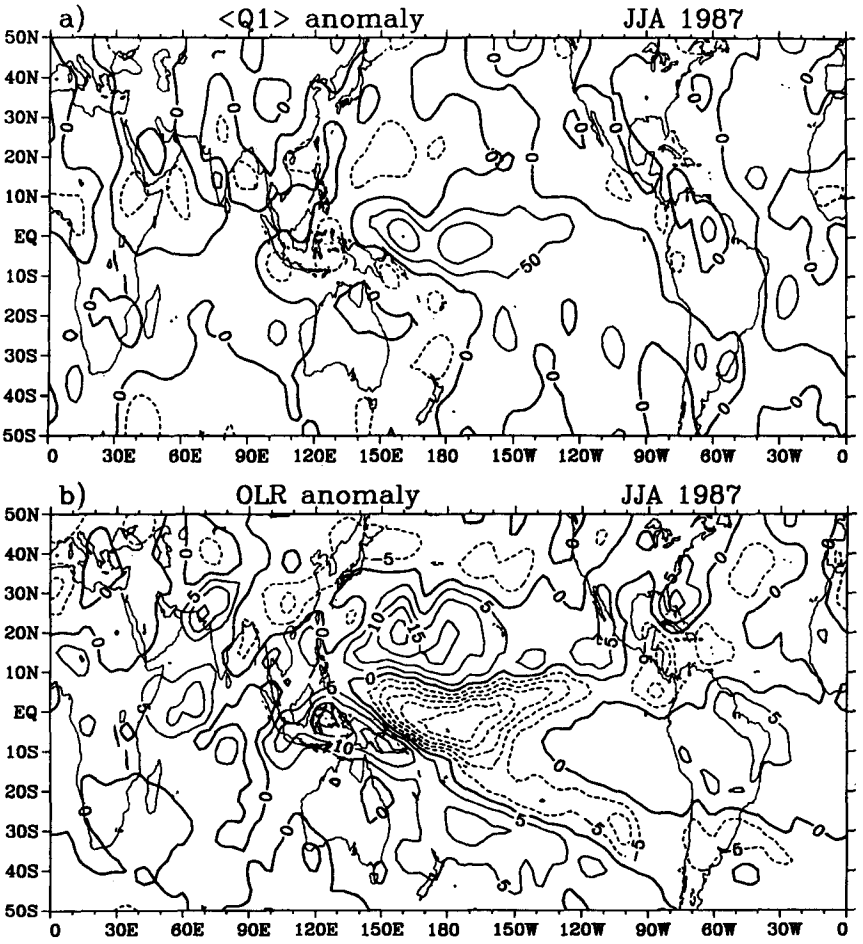


FIG. 16. As in Fig. 15 but for summer 1987.

anic circulations in the tropical Pacific leads the anomalous Asian summer monsoon circulation (e.g., Rasmusson and Carpenter 1983; Shukla and Paolino 1983). Joseph et al. (1994) discussed the interannual variability of the onset of the Indian summer monsoon and its association with El Niño and SST anomalies. Moreover, several recent studies (e.g., Eliott and Angell 1987; Yasunari 1987, 1990, 1991; Yasunari and Seki 1992; Webster and Yang 1992) suggest that the Asian summer monsoon may play an active role in its interaction with ENSO. We need to examine the dynamical linkage between the Asian summer monsoon and various circulation features. We also need to quantify the relative significance of the SST and heat source variations in the framework of land–sea thermal contrast.

4) Our study demonstrated that the variability of the Asian summer monsoon is clearly associated with the variability of the thermal contrast between Eurasia and the Pacific and Indian Oceans. This gives an observational support to recent results of a GCM sensitivity experiment (Meehl 1994a), and suggests the importance of the processes over land for the dynamics of monsoon. Yanai and Li (1994a) have discussed the diurnal variation of the deep mixed layer on the Tibetan Plateau and its possible roles in the tropospheric heating. Smith and Shi (1992) and Shi and Smith (1992) discussed the possible reduction of the net radiative cooling rates over the Plateau because of extremely high surface skin temperature. In view of the crucial role of sensible heating over the Tibetan Plateau region in spring, the impact of snow cover on the heat budget of the land surface (e.g., Hahn and Shukla 1976; Dickson 1984; Yasunari et al. 1991) needs to be studied further. There is a suggestion that excessive Eurasian snow cover in winter and spring may lead to not only a weaker summer monsoon but also weaker trade winds in the tropical Pacific Ocean, which possibly trigger an ENSO event (e.g., Barnett et al. 1989; Vernekar et al. 1995). Recently, Yanai and Li (1994b) found the presence of three conspicuous spectral peaks at ENSO (3–6 years), quasi-biennial, and near 15-month periodicity not only in the monsoon intensity and SST (e.g., Lau and Sheu 1988; Rasmusson et al. 1990) but also in

Eurasian snow cover. These suggest interesting land–atmosphere–ocean interactions.

*Acknowledgments.* The authors thank two anonymous reviewers for their constructive comments on the first version of this paper. This work was supported by the National Science Foundation under Grants ATM-9114229 and ATM9500338, and by the National Oceanic and Atmospheric Administration under Grant NA56GP0203. The computations were performed at computing facilities at NCAR/Scientific Computing Division, and the Office of Academic Computing and the Department of Atmospheric Sciences at University of California, Los Angeles.

APPENDIX A

## Computation of $\omega$

In this study, the vertical $p$ velocity $\omega$ is recomputed from the horizontal divergence by vertically integrating the continuity equation

$$\frac{1}{a\cos\phi}\left[\frac{\partial u}{\partial\lambda}+\frac{\partial}{\partial\phi}(v\cos\phi)\right]+\frac{\partial\omega}{\partial p}=0 \quad \text{(A1)}$$

with the surface boundary condition

$$\omega=\omega_s=-g\rho_s\left(\frac{u_s}{a\cos\phi}\frac{\partial h}{\partial\lambda}+\frac{v_s}{a}\frac{\partial h}{\partial\phi}\right) \quad \text{at} \quad p=p_s. \quad \text{(A2)}$$

In (A1) and (A2) $u$ and $v$ are the zonal and meridional components of the horizontal wind, $a$ the mean earth radius, $\lambda$ the longitude, $\phi$ the latitude, $g$ the acceleration of gravity, $\rho$ the air density, and $h$ the terrain height. The suffix $s$ denotes the surface value. The values of smoothed terrain height are taken from the NMC FGGE Level IIIa data tape.

To reduce errors in estimates of heating rates in the upper troposphere, we impose an additional condition,

$$\omega=\omega_T=-\frac{\left(\frac{\partial\theta}{\partial t}+\mathbf{V}\cdot\nabla\theta\right)}{\left(\frac{\partial\theta}{\partial p}\right)} \quad \text{at} \quad p=p_T. \quad \text{(A3)}$$

Monthly mean values of the tropopause pressure $p_T(\lambda, \phi)$ are obtained from the objectively analyzed tropopause level pressure data during FGGE (see Yanai et al. 1992 for further details). The original estimates of the horizontal divergence, $D_0$, are adjusted by adding

$$D'=\frac{\left(\omega_T-\omega_s-\int_{p_T}^{p_s}D_0\,dp\right)}{(p_s-p_T)}. \quad \text{(A4)}$$

Then the corrected divergence, $D=D_0+D'$, is used in (A1) to obtain $\omega$.

APPENDIX B

## Indices of Monsoon Intensity

We compared four indices to measure the intensity of the Asian summer monsoon. In summer the southwesterlies at lower levels and the northeasterlies at upper levels prevail over the Asian monsoon region. The flows reverse their directions in winter. Two indices were considered to represent the intensity of the broad-scale monsoon circulation. The first is the vertical shear of zonal wind between 850 and 200 hPa, defined by (7) and averaged over the region (0°–20°N; 40°–110°E) (see Fig. 1). This index was used by Webster and Yang (1992). The readers are referred to their paper for further details.

The second index of monsoon circulation is defined by

$$S_2=u_{sw}(850\text{ hPa})-u_{sw}(200\text{ hPa}), \quad \text{(B1)}$$

where $u_{sw}$ is the projection of wind vector in the direction of southwest–northeast. Here $u_{sw}$ can be obtained by $u_{sw}=(u+v)/\sqrt{2}$; $S_2$ was also averaged over summer months and over the same region.

The OLR flux can be used to define the intensity of convection associated with the summer monsoon. We defined the OLR index as the mean OLR averaged over South Asia (10°–25°N; 70°–120°E). In this region the mean OLR values are greater than 260 W m$^{-2}$ (i.e., free of cumulus convection) in winter, but smaller than 240 W m$^{-2}$ (i.e., tall cumulus clouds) in summer. The annual cycle and considerable interannual variability of convective activity can be clearly identified using this index.

The last quantity tested is summer months precipitation amounts averaged over the Indian subcontinent. Many authors used precipitation amounts to categorize the strength of the monsoon (e.g., Mooley and Shukla 1987; Meehl 1987; Krishnamurti et al. 1989). But precipitation is highly affected by orography and localized phenomenon. The Asian summer monsoon is a global-scale phenomenon and the Indian subcontinent is only a small part of the area under the influence of the summer monsoon. Therefore, the use of the Indian summer rainfall amounts alone as a measure of the Asian summer monsoon intensity does not seem to be appropriate.

Figure B1 shows the summer anomalies of $S_1$, $S_2$, the OLR flux and all-Indian summer rainfall (Sontakke et al. 1993) from the 14-yr (1979–1992) means. The behaviors of $S_1$ and $S_2$ are found to be very similar (correlation coefficient 0.96). Correlations between the OLR flux, and $S_1$ and $S_2$ are negative and fairly strong (−0.55 and −0.52, respectively). Correlations between the all-Indian summer rainfall, and $S_1$ and $S_2$ are positive but very weak (0.13 and 0.15, respectively). The correlation between the OLR field and the Indian summer rainfall is found to be rather weak (−0.28).

The year 1988 is classified as a strong monsoon year in terms of the Indian monsoon rainfall (Fig. B1d), and

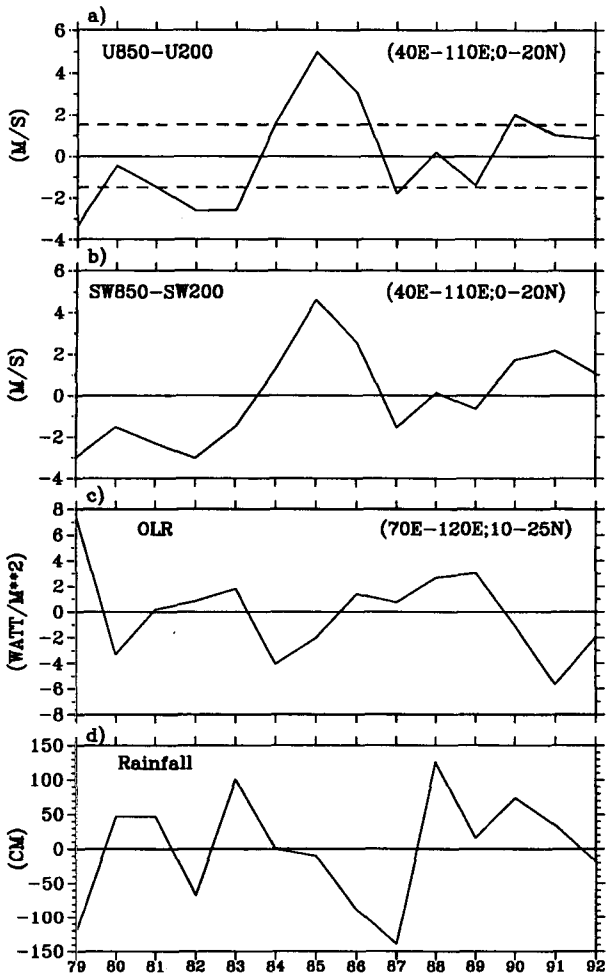


FIG. B1. Summer mean anomalies of $S_1$, $S_2$, OLR index, and all-Indian summer monsoon rainfall from the 14-yr (1979–1992) mean values.

was used as a typical example of a strong monsoon in the Monsoon Numerical Experimentation Group related studies (e.g., Palmer et al., 1992; Meehl 1994b). However, 1988 is near average in terms of the monsoon circulation indices $S_1$ and $S_2$ (Figs. B1a,b). The year 1987 is classified as a weak monsoon year in terms of both the Indian monsoon rainfall and the monsoon circulation indices. The year 1985 shows up as the strongest monsoon in $S_1$ and $S_2$, but is slightly below average for the Indian monsoon rainfall.

Although there is no absolute way to judge which quantity is best to define the intensity of the Asian summer monsoon, we follow Webster and Yang (1992) to choose $S_1$ as the index of monsoon intensity to classify the monsoon seasons into strong and weak monsoon seasons. Here $S_1$ is thought to represent the intensity of broad-scale Asian summer monsoon circulation and also correlated fairly well with the OLR index.

## REFERENCES


Angell, J. K., 1981: Comparison of variations in atmospheric quantities with sea surface temperature variations in the equatorial eastern Pacific. *Mon. Wea. Rev.*, **109,** 230–243.

Barnett, T. P., 1983: Interaction of the monsoon and Pacific trade wind system at interannual time scales. Part I: The equatorial zone. *Mon. Wea. Rev.*, **111,** 756–773.

——, 1984a: Interaction of the monsoon and Pacific trade wind system at interannual time scales. Part II: The tropical band. *Mon. Wea. Rev.*, **112,** 2380–2387.

——, 1984b: Interaction of the monsoon and Pacific trade wind system at interannual time scales. Part III: A partial anatomy of the Southern Oscillation. *Mon. Wea. Rev.*, **112,** 2388–2400.

——, L. Dümenil, U. Schlese, E. Roeckner, and M. Latif, 1989: The effect of Eurasian snow cover on regional and global climate variations. *J. Atmos. Sci.*, **46,** 661–685.

Bhalme, H. N., and D. A. Mooley, 1980: Large-scale droughts/floods and monsoon circulation. *Mon. Wea. Rev.*, **108,** 1197–1211.

Dickson, R. R., 1984: Eurasian snow cover versus Indian monsoon rainfall—an extension of the Hahn–Shukla results. *J. Climate Appl. Meteor.*, **23,** 171–173.

Elliot, W. P., and J. K. Angel, 1987: The relation between Indian monsoon rainfall, the Southern Oscillation, and hemispheric air and sea temperature: 1884–1994. *J. Climate Appl. Meteor.*, **26,** 943–948.

Flohn, H., 1957: Large-scale aspects of the "summer monsoon" in South and East Asia. *J. Meteor. Soc. Japan,* 75th Ann. Vol., 180–186.

——, 1960: Recent investigations on the mechanism of the "summer monsoon" of southern and eastern Asia. *Monsoons of the World.* The Manager of Publications, Delhi, India, 75–88.

Fu, C., and J. O. Fletcher, 1985: The relationship between Tibet-tropical ocean thermal contrast and interannual variability of Indian monsoon rainfall. *J. Climate Appl. Meteor.*, **24,** 841–847.

Gao, Y.-X., M.-C. Tang, S.-W. Luo, Z.-B. Shen, and C. Li, 1981: Some aspects of recent research on the Qinghai-Xizang Plateau meteorology. *Bull. Amer. Meteor. Soc.*, **62,** 31–35.

Hahn, D. J., and J. Shukla, 1976: An apparent relationship between Eurasian snow cover and Indian monsoon rainfall. *J. Atmos. Sci.*, **33,** 2461–2462.

He, H., J. W. McGinnis, Z. Song, and M. Yanai, 1987: Onset of the Asian monsoon in 1979 and the effect of the Tibetan Plateau. *Mon. Wea. Rev.*, **115,** 1966–1995.

Hoskins, B. J., H. H. Hsu, I. N. James, M. Masutani, P. D. Sardeshmukh, and G. H. White, 1989: Diagnostics of the global atmospheric circulation based on ECMWF analyses 1979–1989. World Climate Research Programme-27, WMO/TD-326, 217 pp.

Johnson, D. R., R. D. Townsend, and M.-Y. Wei, 1985: The thermally coupled response of the planetary scale circulation to the global distribution of heat sources and sinks. *Tellus,* **37A,** 106–125.

Joseph, P. V., J. K. Eischeid, and R. J. Pyle, 1994: Interannual variability of the onset of the Indian summer monsoon and its association with atmospheric features, El Niño, and sea surface temperature anomalies. *J. Climate,* **7,** 81–105.

Krishnamurti, T. N., 1985: Summer Monsoon Experiment—a review. *Mon. Wea. Rev.*, **113,** 1590–1626.

——, H. S. Bedi, and M. Subramaniam, 1989: The summer monsoon of 1987. *J. Climate,* **2,** 321–340.

——, ——, and ——, 1990: The summer monsoon of 1988. *Meteor. Atmos. Phys.*, **42,** 19–37.

Lau, K.-M., and P. J. Sheu, 1988: Annual cycle, quasi-biennial oscillation, and Southern Oscillation. *J. Geophys. Res.*, **93,** 10 975–10 988.

Li, C., 1994: Interannual variability of the Asian summer monsoon and its relationships with ENSO and Eurasian snow cover. Ph.D. dissertation, University of California, Los Angeles, 197 pp.

Luo, H., and M. Yanai, 1984: The large-scale circulation and heat sources over the Tibetan Plateau and surrounding areas during the early summer of 1979. Part II: Heat and moisture budgets. *Mon. Wea. Rev.*, **112,** 966–989.

Meehl, G., 1987: The annual cycle and interannual variability in the tropical Pacific and Indian Ocean region. *Mon. Wea. Rev.*, **115,** 27–50.

——, 1994a: Influence of the land surface in the Asian summer monsoon: External conditions versus internal feedbacks. *J. Climate,* **7,** 1033–1049.

——, 1994b: Coupled land–ocean–atmosphere processes and South Asian monsoon variability. *Science,* **266,** 263–267.

Mooley, D. A., and J. Shukla, 1987: Variability and forecasting of the summer monsoon rainfall over India. *Monsoon Meteorology,* C. P. Chang and T. N. Krishnamurti, Eds., Oxford University Press, 26–59.

Murakami, T., 1987: Effects of the Tibetan Plateau. *Monsoon Meteorology,* C.-P. Chang and T. N. Krishnamurti, Eds., Oxford University Press, 235–270.

——, and Y.-H. Ding, 1982: Wind and temperature changes over Eurasia during the early summer of 1979. *J. Meteor. Soc. Japan,* **60,** 183–196.

——, and T. Nakazawa, 1985: Transition from the Southern to Northern Hemisphere summer monsoon. *Mon. Wea. Rev.*, **113,** 1470–1486.

——, and J. Matsumoto, 1994: Summer monsoon over the Asian continent and western North Pacific. *J. Meteor. Soc. Japan,* **72,** 719–745.

Nitta, T., 1983: Observational study of heat sources over the eastern Tibetan Plateau during the summer monsoon. *J. Meteor. Soc. Japan,* **61,** 590–605.

Palmer, T. N., C. Brankovic, P. Vierbo, and M. J. Miller, 1992: Modeling interannual variations of summer monsoons. *J. Climate,* **5,** 399–417.

Parthasarathy, B., and D. A. Mooley, 1978: Some features of a long homogeneous series of Indian summer rainfall. *Mon. Wea. Rev.*, **106,** 771–781.

Rasmusson, E. M., and T. H. Carpenter, 1983: The relationship between the eastern Pacific sea surface temperature and rainfall over India and Sri Lanka. *Mon. Wea. Rev.*, **111,** 517–528.

——, X. Wang, and C. F. Ropelewski, 1990: The biennial component of ENSO variability. *J. Mar. Syst.*, **1,** 71–96.

Schaack, T. K., and D. R. Johnson, 1994: January and July global distributions of atmospheric heating for 1986, 1987, and 1988. *J. Climate,* **7,** 1270–1285.

——, and ——, M.-Y. Wei, 1990: The three-dimensional distribution of atmospheric heating during the GWE. *Tellus,* **42A,** 305–327.

Shi, L., and E. A. Smith, 1992: Surface forcing of the infrared cooling profile over the Tibetan Plateau. Part II: Cooling-rate variation over large-scale plateau domain during summer monsoon transition. *J. Atmos. Sci.*, **49,** 823–844.

Shukla, J., and D. A. Paolino, 1983: The Southern Oscillation and long-range forecasting of the summer monsoon rainfall over the India. *Mon. Wea. Rev.*, **111,** 1830–1837.

Smith, E. A., and L. Shi, 1992: Surface forcing of the infrared cooling profile over the Tibetan Plateau. Part I: Influence of relative longwave radiative heating at high altitude. *J. Atmos. Sci.*, **49,** 805–822.

Sontakke, N. A., G. B. Pant, and N. Singh, 1993: Construction of all-India summer monsoon rainfall series for the period 1844–1991. *J. Climate,* **6,** 1807–1811.

Trenberth, K. E., 1992: Global analyses from ECMWF and atlas of 1000 to 10 mb circulation statistics. NCAR Tech. Note, NCAR/TN-373+STR, 191 pp.

——, and J. G. Olson, 1988: ECMWF global analyses 1979–86: Circulation statistics and data evaluation. NCAR Tech. Note, NCAR/TN–300+STR, 94 pp.

——, and A. Solomon, 1994: The global heat balance: Heat transports in the atmosphere and ocean. *Climate Dyn.*, **10,** 107–134.

Vernekar, A. D., J. Zhou, and J. Shukla, 1995: The effect of Eurasian snow cover on the Indian monsoon. *J. Climate,* **8,** 248–266.

Webster, P. J., and S. Yang, 1992: Monsoon and ENSO: Selectively interactive systems. *Quart. J. Roy. Meteor. Soc.*, **118,** 877–926.

Wei, M.-Y., D. R. Johnson, and R. D. Townsend, 1983: Seasonal distributions of diabatic heating during the First GARP Global Experiment. *Tellus,* **35A,** 241–255.

Yanai, M., and C. Li, 1994a: Mechanism of heating and the boundary layer over the Tibetan Plateau. *Mon. Wea. Rev.*, **122,** 305–323.

——, and ——, 1994b: Interannual variability of the Asian summer monsoon and its relationship with ENSO, Eurasian snow cover and heating. *Proc. Int. Conf. on Monsoon Variability and Prediction.* Trieste, Italy, WMO/TD No. 619, Vol. I, 27–34.

——, S. Esbensen, and J.-H. Chu, 1973: Determination of bulk properties of tropical cloud clusters from large-scale heat and moisture budgets. *J. Atmos. Sci.*, **30,** 611–627.

——, C. Li, and Z. Song, 1992: Seasonal heating of the Tibetan Plateau and its effects on the evolution of the Asian summer monsoon. *J. Meteor. Soc. Japan,* **70,** 319–351.

Yasunari, T., 1987: Global structure of the El Niño/Southern Oscillation. Part II: Time evolution. *J. Meteor. Soc. Japan,* **65,** 81–102.

——, 1990: Impact of Indian monsoon on the coupled atmosphere/ocean system in the tropical Pacific. *Meteor. Atmos. Phys.*, **44,** 29–41.

——, 1991: "The monsoon year"—a new concept of the climatic year in the Tropics. *Bull. Amer. Meteor. Soc.*, **72,** 1331–1338.

——, and Y. Seki, 1992: Role of the Asian monsoon on the interannual variability of the global climate system. *J. Meteor. Soc. Japan,* **70,** 177–189.

——, A. Kitoh, and T. Tokioka, 1991: Local and remote responses to excessive snow mass over Eurasia appearing in the northern spring and summer climate—a study with the MRI-GCM. *J. Meteor. Soc. Japan,* **69,** 473–487.

Ye, D., 1981: Some characteristics of the summer circulation over the Qinghai-Xizang (Tibet) Plateau and its neighborhood. *Bull. Amer. Meteor. Soc.*, **62,** 14–19.

——, and Y.-X. Gao, 1979: *The Meteorology of the Qinghai-Xizang (Tibet) Plateau* [in Chinese]. Science Press, 278 pp.